Preprint Title	Influence of conductive carbon content in hydrogel-based composite on morphological and electrical properties for electrochemical energy conversion
Authors	Sylwia Pawłowska, Karolina Cysewska, Yasamin Ziai, Jakub Karczewski, Piotr Jasiński and Sebastian Molin
Publication Date	13 Juli 2023
Article Type	Full Research Paper
ORCID® iDs	Sylwia Pawłowska - https://orcid.org/0000-0002-3700-7885

Influence of conductive carbon content in hydrogel-based composite on morphological and electrical properties for electrochemical energy conversion

Sylwia Pawłowska*[1], Karolina Cysewska[1], Yasamin Ziai[2], Jakub Karczewski[3], Piotr Jasiński[1] and Sebastian Molin[1]

[1] Faculty of Electronics, Telecommunications and Informatics, and Advanced Materials Center, Gdańsk University of Technology, G. Narutowicza St. 11/12, 80-233 Gdańsk, Poland

[2] Institute of Fundamental Technological Research, Polish Academy of Sciences, Pawińskiego St. 5B, 02-106 Warsaw, Poland

[3] Faculty of Applied Physics and Mathematics, and Advanced Materials Center, Gdańsk University of Technology, G. Narutowicza St. 11/12, 80-233 Gdańsk, Poland

Email: Sylwia Pawłowska - sylwia.pawlowska@pg.edu.pl

* Corresponding author

Abstract

In this work, a strategy for the one-stage synthesis of polymer composites based on PNIPAAm hydrogel was presented. Both conductive particles in the form of conductive carbon black (cCB) and $MnCo_2O_4$ (MCO) spinel particles were suspended in the three-dimensional structure of the hydrogel. The MCO particles in the resulting hydrogel composite acted as an electrocatalyst in the OER process. Morphological studies confirmed that the added particles were incorporated and, in the case of a higher

concentration of cCB particles, also bound to the surface of the structure of the hydrogel matrix. The produced composite materials were tested in terms of their electrical properties, showing that an increase in the concentration of conductive particles in the hydrogel structure translates into a lowering of the impedance modulus and an increase in the double-layer capacitance of the electrode. This, in turn, resulted in a higher catalytic activity of the electrode in the OER reaction. The use of a hydrogel as a matrix to suspend the catalyst particles, and thus increase their availability through the electrolyte, seems to be an interesting and promising application approach.

Keywords

polymer composites; energy; hydrogen; electrical properties; oxygen evolution reaction

Introduction

Hydrogels are defined as a group of polymeric materials with an insoluble hydrophilic structure that gives them the ability to absorb and hold large amounts of water (up to over 99 wt%) in their three-dimensional network. The phenomenon of hydrogels swelling in the water while not dissolving in it is due to the hydrophilic functional groups attached to the polymer backbone and the cross-links between the network chains. High water content makes hydrogel materials similar in terms of microstructure and flexibility to living tissues. The amount of water absorbed depends on such factors as the structure of the hydrogel, the composition of the precursor hydrogel solution, the cross-link density, and the technique of its synthesis. The simple reaction of one or more monomers is used for the production of this kind of material [1-3]. The methods of synthesising hydrogels are divided into two basic groups, including physical and chemical cross-linking. Physical crosslinking methods, which are mainly related to the

synthesis of natural hydrogels, include changes in intermolecular interactions, for example, hydrophobic interactions, ionic cross-linking, and hydrogen-bonded gels. Chemically synthesised hydrogels are produced by covalent cross-linking pathways such as radical polymerisation, radiation cross-linking, grafting, thermo-gelation, enzymatic reactions, and click chemistry [4, 5].

Hydrogel materials have quite a long history and a wide range of applications, especially in biology, medicine, tissue engineering, and pharmacy. The multitude of application areas is related to their exceptional properties: biocompatibility, biodegradability, nontoxicity, good permeability for substances dissolved in the water, such as oxygen and metabolites, flexibility with high mechanical strength, chemical and thermal resistance, high rate of reversible fluid absorption, and low interfacial tension with water [6, 7]. A very desirable property of hydrogels is the ability to incorporate or suspend various particles in their structure, such as dyes, drugs, metal nanoparticles, metal oxide nanoparticles, and carbon nanotubes, as well as drugs or biomolecules. This is a very important advantage that opens ways of designing composite hydrogel materials with various properties and applications such as biomedical [8-10], biosensors [11-13], wearable electronics [14-16], and environment [17, 18]. In recent years, scientists have been very interested in the use of hydrogels in the process of electrocatalytic water splitting to produce hydrogen from renewable energy sources. These studies assume the use of empty spaces, thus ensuring efficient mass transport, as well as increasing electrochemically active surfaces. The great advantage of the 3D hydrogel structure is the increase of the catalytic surface area thanks to the possibility of conducting the electrochemical reaction deeper into the structure of the hydrogel. This structure is designed to facilitate and increase mass transport; therefore, it is vital to achieve the desired three-dimensional structure of the material. In addition, the free space in the form of pores and network structure within

the morphology facilitates the penetration by the electrolyte, the diffusion of ions to electroactive sites, and the rapid release of the reaction, thus promoting the kinetics of the reaction and achieving higher efficiency of the catalyst built into the hydrogel structure [19, 20]. The condition which must be met for hydrogel materials to be used in energy conversion systems is their appropriate electrical conductivity [21]. Suspension of conductive fillers in the hydrogel structure such as metallic particles (gold nanoparticles, silver nanoparticles) [22-24], carbon-based materials (GO graphene oxide, CNT carbon nanotubes) [25-27], and conductive polymers (polyaniline, polypyrrole, and poly-ethylenedioxythiophene) [28-30], allows for the formation of conductive hydrogels. Conducting hydrogels possess the properties of both conductive polymers and hydrogels, which make them attractive functional materials for many applications in several fields of science and technology such as environmental engineering [31], renewable energy [32-35], electronics [36-38], medical devices [39-41], and drug delivery systems [42-45]. They combine the properties of a hydrophilic matrix with conductive properties obtained thanks to the use of an appropriate conductive component at the stage of hydrogel synthesis. Hydrogel matrices are an excellent medium for depositing metallic nanocatalysts, especially in reactions requiring aqueous media such as electrochemical processes. The dispersion of the catalyst particles in the hydrogel helps to avoid or significantly reduce the formation of aggregates, increase the active surface area of the catalyst, and thus affects its efficiency [46].

In this work, we suspended particles of the $MnCo_2O_4$ electrocatalyst and conductive carbon in a PNIPAAm hydrogel precursor solution, which was then subjected to the polymerisation process. As a result, a hydrogel composite was created in a single-stage synthesis process. In addition, the applied methodology allowed us to avoid the need to use elevated temperature at the synthesis stage, which is an essential step in

most of the conventional synthesis paths of conductive hydrogels described in the literature [22, 23, 25-27]. These two features, the one-stage process, and the low-temperature needed, are used for synthesising the polymer composite with significant electrical conductivity resulting from the presence of conductive carbon particles in a process that is much faster and easier to perform. It is also cheaper, as it does not require electricity consumption in the process of several hours of mixing and/or heating. The produced hydrogel structures were examined in terms of their morphology, electrical properties, and catalytic layers in the OER process.

Results and Discussion

Characterisation of hydrogel-based polymer composites with dispersed catalytic and conductive particles

High-resolution SEM analysis of the hydrogel samples subjected to the lyophilisation process was performed to determine the presence of catalyst particles and conductive carbon on the surface of the porous skeleton created by the PNIPAAm polymer. Figures 1a and Figure 1d show a porous structure, with pure hydrogel as the skeleton. Higher magnification of the polymer surface for the sample Hgel-MCO-cCB 1:3 showed the presence of MCO and cCB particles in the hydrogel scaffold, confirming their entrapment in the polymer matrix (Figures 1b, 1e). A similar composite structure with gold nanorods suspended in the PNIPAAm matrix was observed by Nakielski et al. [50]. Cai et al. found some silver nanoparticles only slightly present in the skeleton of PVA@DEL composite hydrogel [22]. Most of the Ag nanoparticles were observed in the wall of the hydrogel network. In our case, for the Hgel-MCO-cCB 1:3 sample, when the volume percentage of cCB was 17.1%. (Table 1), the particles of conductive carbon and catalyst were incorporated into the structure of the hydrogel matrix. Increasing the

volumetric contribution of cCB particles above this value (for example, for the Hgel-MCO-cCB 1:6 sample) resulted in the partial release of these particles onto the surface of the polymer matrix (Figure 1c, 1f). However, the samples were not homogeneous in terms of the distribution of the composite particles in the hydrogel structure. Even at high concentrations of conductive particles, there were regions where the hydrogel skeleton was covered with cCB particles, while inside the backbone, very few of them were observed. Therefore, it can be concluded that there is a certain limit to the concentration of particles added to the hydrogel, which after the polymerisation process are trapped in the hydrogel skeleton. Above this limit, excess particles are still bound to the polymer scaffold, coating its surface. The characteristic porous structure is still formed but has a much more granular structure. The presence of the pores is very important in the case of the application of hydrogel composite in oxygen evolution reaction. As was maintained above, the porosity has a beneficial effect on the diffusion of electrolytes in an electrochemical process. It provides a greater effective surface area and facilitates the transport of electrons and ions from the electrolyte to the electrocatalyst surface. As the morphological analysis showed, with the increase in the concentration of conductive carbon particles, the size of the pores and their number decreases. Further research should focus, among others, on finding the right proportions between the components of hydrogel composites to achieve a balance between the influence of porosity and conductive properties of these composites on the electrochemical activity of catalyst particles in the OER process.

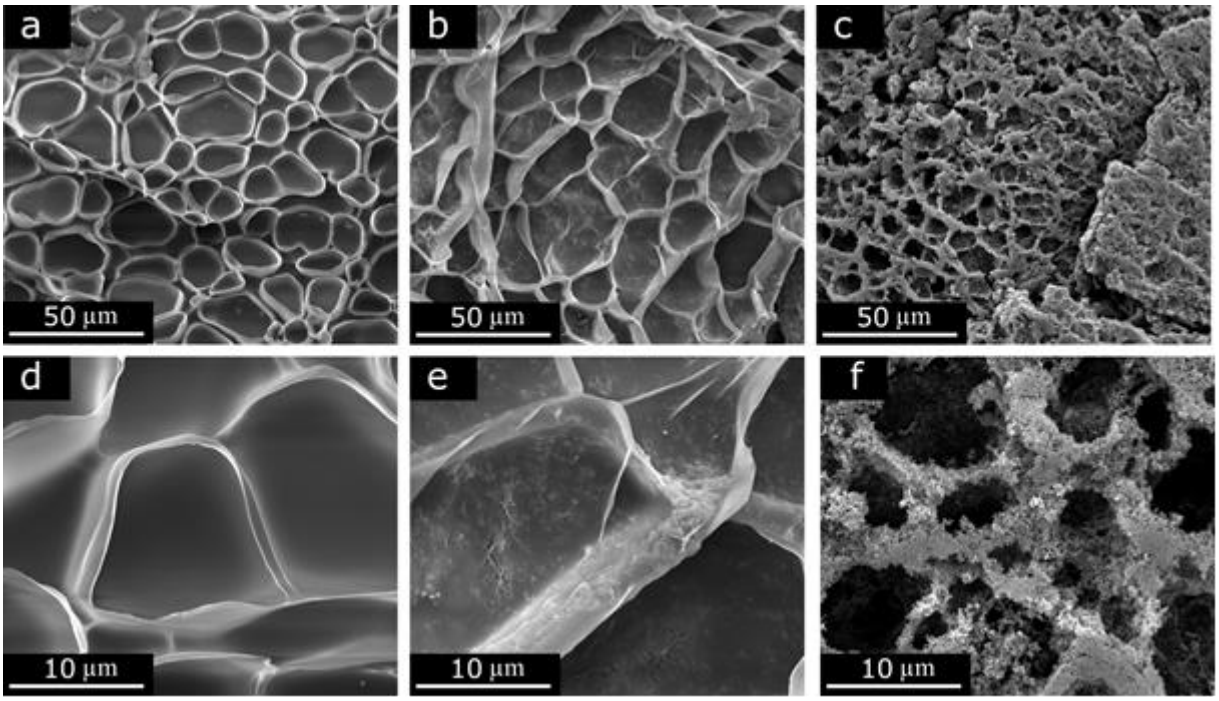

Figure 1: SEM micrographs of freeze-dried nanostructures of pure (a, d) and composite hydrogel samples: Hgel-MCO-cCB 1:3 (b, e) and Hgel-MCO-cCB 1:6 (c, f).

Elemental mapping (EDS) confirmed the presence of MCO particles inside the hydrogel structure (Figure 2). It was not possible to detect the presence of conductive carbon (cCB) particles both due to the limitations of the instruments and the presence of carbon atoms also in the polymer chains forming the hydrogel skeleton. As mentioned above, the higher the concentration of cCB, the more MCO catalyst particles are also outside the surface of the polymer scaffold. In addition, it can be concluded that in the case of a hydrogel sample with Hgel-MCO catalyst particles (Figures 2a, 2d, 2g), the dispersion of these particles is quite poor and MCO aggregates were visible. With the increase in the concentration of particles added to the hydrogel, the number of visible aggregates of MCO particles decreases (Figures 2b, 2c, 2e, 2f, 2h, 2i). In the case of a sample where the concentration of particles of conductive carbon cCB reached the value of 54.6 mg/mL (Hgel-MCO-cCB 1:6), much smaller MCO aggregates were visible (Figures 2c, 2f, 2i). The average diameter of the

used commercial $MnCo_2O_4$ particles after 0.5 hours in an ultrasound bath was 204.5±92.9 nm [48]. Also, their arrangement seems to be much more homogeneous than in the case of composites with a lower concentration of cCB particles. The dispersion of the catalyst particles in the hydrogel helps to avoid or significantly reduce the formation of aggregates, which may result in an increase of the active surface area of the catalyst, and thus affect its efficiency [46]. Therefore, future research will include the development of a better method of dispersing the MCO and cCB particles in the hydrogel precursor solution to obtain a more homogeneous distribution of these particles in the structure of the polymer matrix and on its surface.

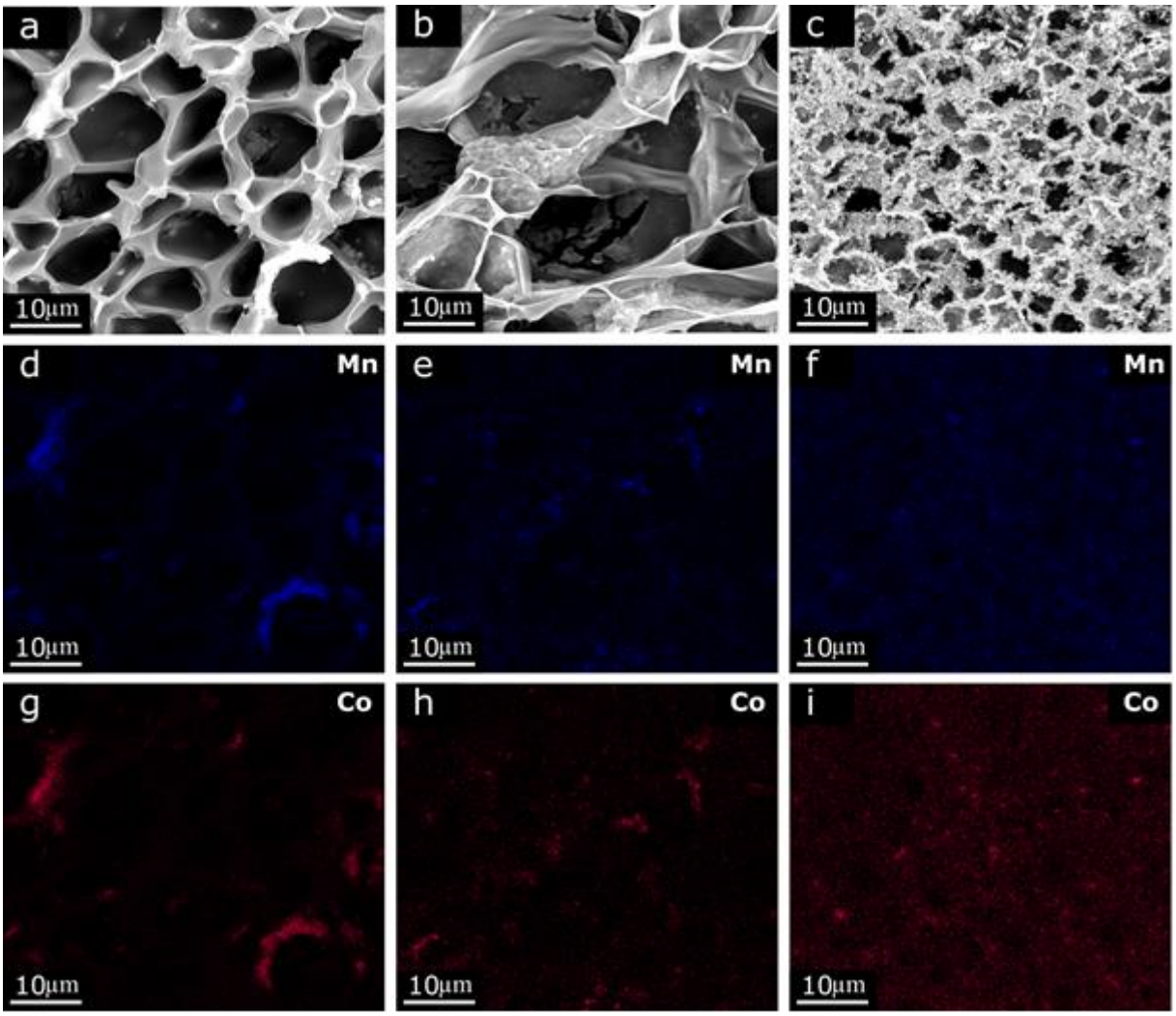

Figure 2: EDS analysis of hydrogel composites: Hgel-MCO (a, d, g), Hgel-MCO-cCB 1:3 (b, e, h), Hgel-MCO-cCB 1:6 (c, f, i).

The FTIR spectra of the hydrogel compositions and their pure components are shown in Figure 3a. Results present the characteristic absorption peaks of PNIPAAm at 3430, 3284, and 3068 cm^{-1}, which are assigned to the N−H stretching of the secondary amine. Peaks at 1637 and 1535 cm^{-1} can be ascribed to the stretching of carbonyl group C=O [42, 51]. In the FTIR spectrum of $MnCo_2O_4$, two absorption bands at 620 and 478 cm^{-1}, characteristic of M-O stretching and vibrations of the spinel structure, were visible (Figure 3b) [52, 53]. In the case of Super P Li Conductive Carbon Black (cCB), no distinct peaks can be seen in the FTIR spectra. However, it is visible that with the increase in the amount of cCB in the structure of the hydrogel, the peaks characteristic of the above-mentioned functional groups forming the hydrogel become less and less intense (Figure 3c). It can therefore be assumed that the high concentration of conductive carbon particles overrides (barriers) signals from other compounds.

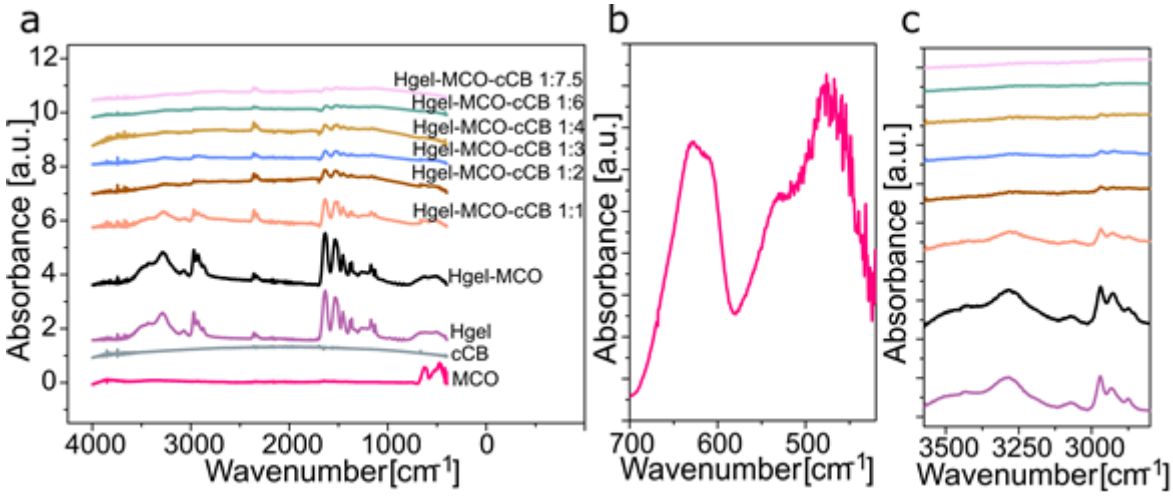

Figure 3: FTIR-ATR spectra of hydrogel composites and their components (a). FT-IR graph of $MnCo_2O_4$ characteristic absorption peaks (b). Comparison of the intensity of P(NIPAAm) characteristic absorption peaks with different conductive carbon black concentrations in hydrogel composite samples (c).

Electrical properties of hydrogel composites

Electrochemical impedance spectroscopy was employed to characterise the electrical properties of the hydrogel-based structures. The impedance modulus |Z| decreased, with the amounts of cCB contained in the hydrogel structure increasing. The changes are within the range of 79.7–1390.5 kΩ at 0.01 Hz and 3.5–18.6 kΩ at 1 Hz. The trend of the EIS graphs shows the capacitive-dominant nature of the hydrogel for all analysed hydrogel-based electrodes. Three different regions were observed in the Bode plots for the hydrogel samples tested. At the highest frequencies (104–103 Hz and 104–102 Hz for samples without and with cCB, respectively), a resistive behaviour is observed (Figure 4a), while the phase shift is close to 0° (Figure 4b). For the hydrogels containing MCO-cCB, the capacitive behaviour starts at 200 Hz, while for the samples without cCB, from 2000 Hz. Depending on the sample, the phase angle reaches a maximum of -90° to -65°. The Nyquist plot (Figure 4c) presented similar profiles for all the samples. In the case of samples without cCB and with cCB content not higher than 36.4 mg/mL, initiation of the semicircular area was observed at higher frequencies, which at lower frequencies did not complete the semi-circle. The two hydrogel samples with the highest cCB contents showed the lowest impedance, as indicated by the smallest diameter of the semi-circles [54]. It is visible that the electrical properties depend strongly on the conductive carbon concentration (Figure 4d). A similar EIS behaviour was observed in the literature for several different hydrogel-based structures [25, 55-57]. For comparison, the impedance values of gelatin methacryloyl (GelMA), GO/GelMA, and r(GO/GelMA) at 1 Hz were 193, 98, and 10 kΩ, respectively [14]. Wu et al. obtained a magnitude of impedance in the range of 3–7 kΩ at 1 Hz for PEGda-PANI hydrogels [55]. Comparable values were obtained for PTAA/MAAG-Based Homogeneous Electronically Conductive Double-Network Hydrogels [56]. These

hydrogel materials were tested for biomedical applications. Nevertheless, they show that the impedance trend obtained by us is similar to other hydrogel materials presented in the literature. Further research will include an impedance analysis of the hydrogel materials and the determination of a model that accurately describes the obtained experimental data.

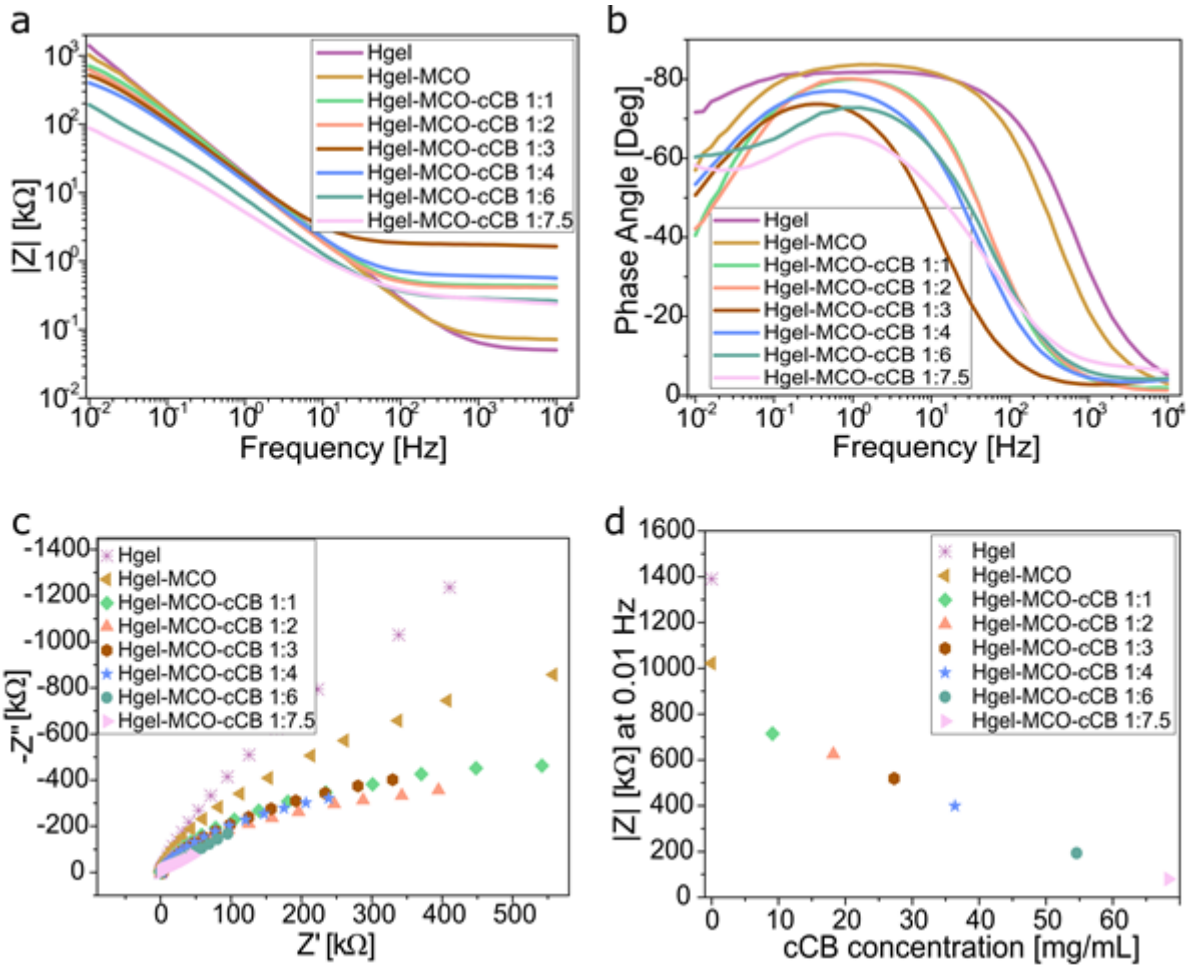

Figure 4: Electrical properties analysis of hydrogel-based samples with catalyst (MCO) and conductive (cCB) particles: a) Bode modulus, b) phase angle, and c) Nyquist plots of hydrogel samples. d) Dependence of the hydrogel |Z| on the cCB concentration at 0.01 Hz.

Application of hydrogel-based composite in oxygen evolution reaction for water splitting

Improvement of the electrical properties resulting from the increase in the amount of conductive carbon particles is also visible in the catalytic activity in the OER (Figure 5). The linear sweep voltammetry polarisation curves (Figure 5a) showed that an increase in the cCB contribution to the hydrogel matrix translated into an increase in the number of conduction paths, as manifested by a higher yield of catalyst particles. The potential required to drive a 10 mA/cm^2 OER current density using the hydrogel with the higher amount of conductive particles compared to catalyst particles (MCO:cCB equal 1:7.5) is 1.73 V versus RHE, which means that the overpotential was 500 mV. Reducing the conducting carbon (MCO: cCB 1:4) by almost half increased the potential to 1.81 V, and thus the overpotential to 630 mV. For samples with a smaller amount of cCB, pure hydrogel, and hydrogel with MCO catalyst, it was impossible to determine the overpotentials at the standard current density value of 10 mA/cm^2. For comparison, the OER activity of the PPy/FeTCPP (polypyrrole/(4-carboxyphenyl)porphyrin hydrogel) and PPy/FeTCPP/Co catalyst at 10 mA/cm^2 current density, and in 0.1 M KOH, were 1.74 and 1.61 versus RHE, respectively (the catalyst loading equal 0.3 mg/cm^2) [58]. Analysis of NF@Hgel-$Fe_{0.3}Co_{0.1}$, NF@Hgel-$Fe_{0.4}$, and NF@Hgel-$Co_{0.4}$ hydrogel catalysts in 1 M KOH for the OER process showed that the overpotential at the current density of 20 mA/cm^2 was 280 mV, 320 mV, and 370 mV, which corresponds to 1.51 V, 1.55 V, and 1.60 V vs RHE, respectively [59]. However, they used more than 4 times the loading of the catalyst (1 mg/cm^2) than we did (0.23 mg/cm^2). Chen et al. obtained overpotential values of 400 mV (corresponds to 1.6 V vs RHE) at 145.3 mA/cm^2 for N-doped graphene hydrogels/NiCo in 0.1 M KOH [33].

The electrode double layer capacitance increased with the increasing cCB particle concentration (Figure 5b). For the pure hydrogel electrode, the double-layer capacitance (C_{dl}) was equal to 0.03 mF/cm^2. The addition of cCB at a proportion of 1:1 with MCO caused the Cdl value to double. The hydrogel electrode, Hgel-MCO-cCB 1:7.5, increased the double-layer capacitance to 1.22 mF/cm^2, and thus increased it over 20 times compared to the Hgel-MCO-cCB 1:1 sample. Tang et al. obtained C_{dl} values of 7.91 mF/cm^2, 9.26 mF/cm^2, and 4.38 mF/cm^2, respectively, for NF@Hgel-$Fe_{0.3}Co_{0.1}$, NF@Hgel-$Fe_{0.4}$, and NF@Hgel-$Co_{0.4}$ electrodes [59], but with 4 times higher catalyst loading.

The catalytic kinetics of the hydrogel samples showed a much lower Tafel slope value for pure hydrogel (141 mV/dec) than those obtained for the hydrogel with catalyst and conductive particles dispersed inside the hydrogel's structure (75–90 mV/dec) (Figure 5c). Depending on the potential applied and the process condition, the water oxidation could be a 1 to 4 electron transfer process [60, 61]. Tafel slope values in the range of 75–90 mV dec^{-1} represent a possible mixed mechanism (2 or 3 electron transfer processes), with a strong influence of 2 electron transfer. Comparing the value of the Tafel slope of the hydrogel composite containing MCO and cCB particles with the Tafel slope of pure hydrogel (141 mV dec^{-1}), it is visible that the addition of the catalyst significantly accelerated the kinetics of the reaction. The increase in the amount of conductive carbon in the structure of the hydrogel composite does not affect the further acceleration of the kinetics, although an increase in catalytic activity is visible, represented by a decrease in overpotential (Figure 5a). This is related to the increase of the electrode double layer capacitance with the increase in the amount of cCB (Figure 5b). This confirms the comparable rate and mechanism of the OER reaction of the Hgel-MCO-cCB electrode. Comparing our Tafel slope with the values obtained for the PPy/FeTCPP and PPy/FeTCPP/Co samples (74 mV/dec and 65 mV/dec,

respectively), they are very similar [58], and much better than the results obtained for NF-NiCo (614 mV/dec) [34]. For transition-metal functionalised polyaniline−phytic acid hydrogels, Tang et al. obtained Tafel slopes in the range of 78–191 mV/dec [59].

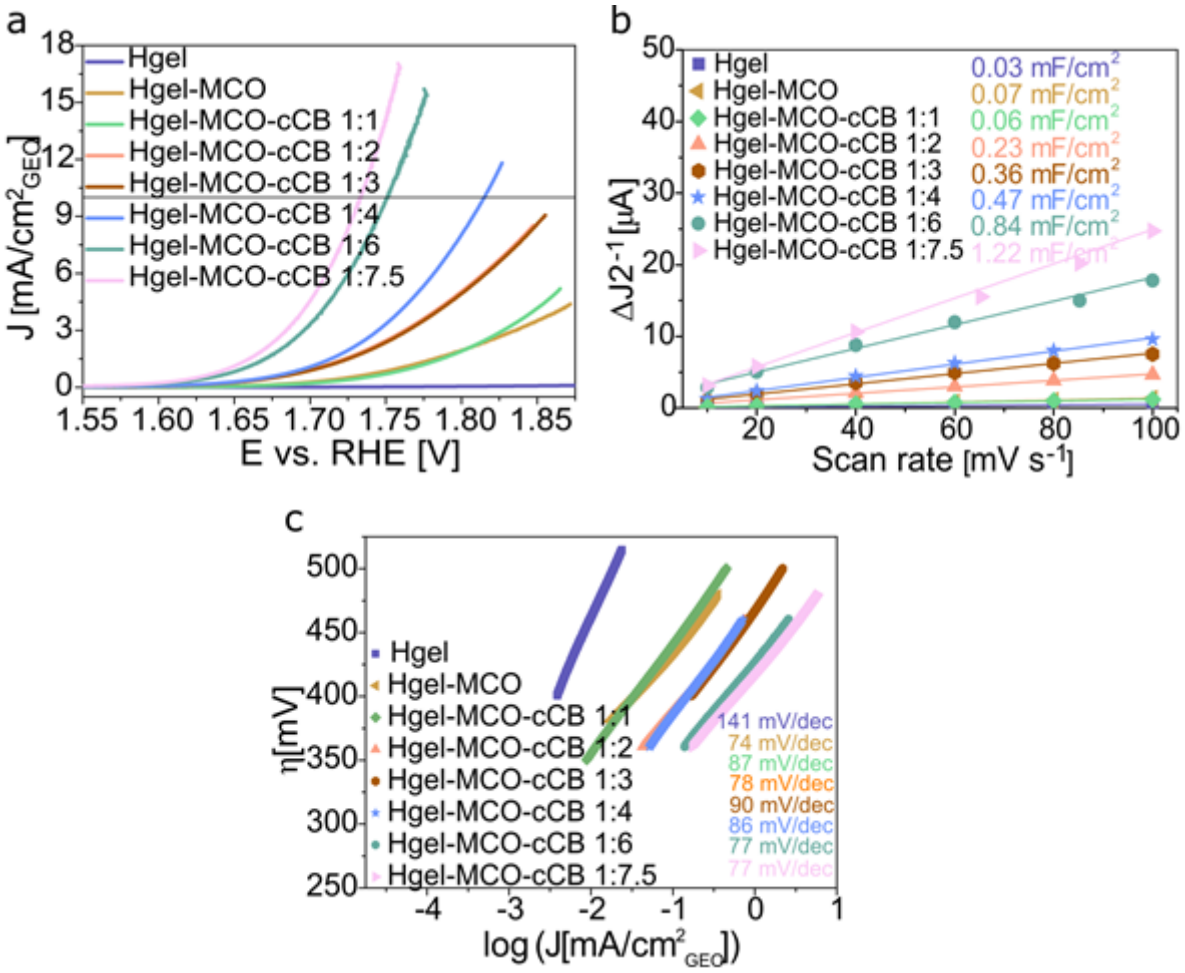

Figure 5: Catalytic activity in the OER process of MCO particles dispersed in the hydrogel: a) polarisation curves, b) double-layer capacitance (C_{dl}), c) Tafel plots.

The results obtained confirm that ensuring the appropriate concentration of ion-conducting and electron-conducting particles in the hydrogel structure is a necessary condition to provide high electrocatalytic efficiency of the catalyst particles participating in the OER process.

Conclusion

The article presents a one-stage method for the fabrication of polymer composites based on a hydrogel in which $MnCo_2O_4$ as a catalyst (MCO) and conductive carbon black (cCB) particles as conductive fillers have been embedded. In the developed method of synthesis, the need to use high temperature was omitted, which is an element that distinguishes the applied procedure from others described in most literature reports. SEM studies confirmed the fabrication of a composite polymer containing MCO catalyst particles and conductive carbon cCB particles caught inside or bound to the surface of the hydrogel. Increasing the concentration of conductive carbon (cCB) particles to a value that prevented their retention in the hydrogel matrix caused MCO and cCB particles to also be present on the surface. After the freeze-drying process, the hydrogel composites were characterised to measure their porosity, as the pores filled with water in the hydrated state will become empty after water sublimation. With the increasing concentration of cCB, the size and number of pores decreased. In the process of electrocatalysis, it is crucial that the size and most importantly, the number of pores, be as large as possible. The porous microstructure of the hydrogel matrix is capable of swelling and thus accommodating significant amounts of an ionic liquid. Such a structure provides constant access of the electrolyte molecules/ions to the catalyst particles surrounding it, increasing the speed and efficiency of the electrochemical reaction. Thereby, efficient electrocatalytic processes are promoted. Using the impedance measurement, we demonstrated the dependency of the electrical properties of the hydrogel on the concentration of conductive particles (cCB) suspended in the three-dimensional structure. In addition, the possibility of using the produced hydrogel composites as electrocatalytic electrodes for the oxygen evolution reaction was presented. The results showed that, as predicted, the higher

the concentration of conductive particles, the higher the electrocatalytic efficiency of the MCO particles. The separation of catalyst particles suspended in the hydrogel and their homogeneous dispersion, combined with the presence of an optimised concentration of conductive particles responsible for the transport of ions and electrons in the hydrogel structure, favour the increase in the efficiency of the OER process. Further work on these types of three-dimensional materials seems to be a promising direction in the search for new active electrodes participating in the water-splitting reaction. The realisation of nanostructured materials plays a key role in the development of the desired materials. Adopting an appropriate strategy for designing hydrogel composites, the method of their production, and modifying their molecular architecture will allow them to meet critical challenges in advanced energy technologies, and overcome the limitations of current materials, improving the efficiency of devices in the field of storage and conversion of energy.

Experimental

Materials

N-isopropylacrylamide (NIPAAm, 97%, Sigma-Aldrich, Poland), N,N′-methylenebisacrylamide (BIS-AAm, 99.5%, Sigma-Aldrich, Poland), 2-hydroxy-4′-(2-hydroxyethoxy)-2-methylpropiophenone (Irgacure 2959, 98%, Sigma-Aldrich, Poland), ammonium persulfate (APS, 98%, Sigma-Aldrich, Poland), N,N,N′,N′-tetramethylethylenediamine (TEMED, 99%, Sigma-Aldrich, Poland), commercially available manganese cobalt spinel $MnCo_2O_4$ powder (MCO, Marion Technologie, France), Super P Li Conductive Carbon Black (cCB, Imerys, Belgium), 0.1 M KOH (Titripur®, Merc, Germany).

Hydrogel sample preparation

Hydrogel with conductive and catalyst particles dispersed throughout was synthesised via a one-step polymerisation procedure – all components were dissolved or suspended in a hydrogel precursor solution (Figure 6). The hydrogel precursor solution was a composition of N-isopropylacrylamide, used as the main monomer (NIPAAm, 97%, Sigma-Aldrich, Poland) and N,N′-methylenebisacrylamide (BIS-AAm, 99.5%, Sigma-Aldrich, Poland) as a cross-linker in the proportion 35:1, dissolved in deionised water (90% wt.). The water solution contained $MnCo_2O_4$ (MCO) as electrocatalyst particles and conductive Carbon Black (cCB) particles as carbon-based conductive fillers. Two types of initiating agents were used in the hydrogel polymerisation process: 2-hydroxy-4′-(2-hydroxyethoxy)-2-methylpropiophenone (Irgacure 2959, 98%, Sigma-Aldrich, Poland) as a photoinitiator used to trigger the hydrogel polymerisation reaction upon UV irradiation, as well as ammonium persulfate (APS, 98%, Sigma-Aldrich, Poland) and N,N,N′,N′-tetramethylethylenediamine (TEMED, 99%, Sigma-Aldrich, Poland). The addition of APS and TEMED was necessary as there is a need to quickly increase the viscosity of the hydrogel precursor solution to avoid the sedimentation of suspended particles (MCO and cCB). Table 1 presents the amounts of each component used in the preparation of the conductive hydrogel samples. UV irradiation (UV EMITA VP-60, 180 W, 220–240V AC) in an ice bath lasted 2–4 minutes for complete polymerisation.

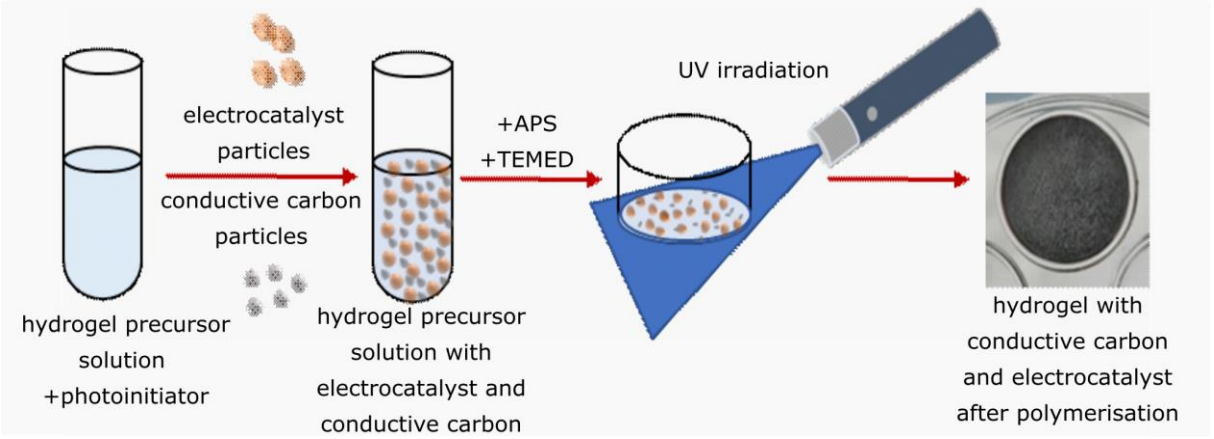

Figure 6: Scheme of hydrogel polymerisation process with electrocatalyst and conductive carbon particles.

Table 1: Composition of hydrogel precursor solutions used for the synthesis of individual samples.

	Sample1 Hgel-MCO	**Sample2 Hgel-MCO-cCB 1:1**	**Sample3 Hgel-MCO-cCB 1:2**	**Sample4 Hgel-MCO-cCB 1:3**	**Sample5 Hgel-MCO-cCB 1:4**	**Sample6 Hgel-MCO-cCB 1:6**	**Sample7 Hgel-MCO-cCB 1:7.5**
NIPAAm	97.2 mg/mL						
BIS-AAm	2.8 mg/mL						
APS	75 µL/mL						
TEMED	7.5 µL/mL						
Irgacure	5 mg/mL						
MCO	9.1 mg/mL						
cCB	-	9.1 mg/mL 5.7% vol	18.2 mg/mL 11.3% vol	27.3 mg/mL 17.1% vol	36.4 mg/mL 22.8% vol	54.6 mg/mL 34.2% vol	68.3 mg/mL 42.8% vol
UV [minute]	2	2	2	3	3	4	4

In contrast to numerous works in which elevated temperature was used for the synthesis of hydrogel composites, here the process of mixing the hydrogel precursor solution with MCO and cCB components in a cooling bath was performed. Similarly, the polymerisation process was performed using a cooling bath to eliminate the high temperature generated by irradiation with a UV lamp. In both cases, we protected the PNIPAAm polymer from reaching the lower critical solution temperature (LCST) by cooling. The LCST of PNIPAM in pure water is about 32°C [47-49]. Polymerisation performed at a temperature above LCST results in shrinkage of the hydrogel structure and the formation of inhomogeneities. Such a hydrogel ceases to be transparent and loses most of its water [42].

Morphological and physicochemical characterisation

SEM analysis was performed with an FEI Quanta FEG 250 scanning electron microscope (FE-SEM) with an accelerating voltage of 10 kV. Before imaging, the hydrogel samples were freeze-dried and coated with a 10 nm gold layer.

The chemical composition of the hydrogel composition was analysed with a Thermo Fisher Scientific Silicon Drift Detector energy dispersive X-ray spectroscope (EDS).

For characterisation of the present material functional groups, FTIR spectroscopy in attenuated total reflectance (ATR) mode was used (Bruker Vertex70 FT-IR Spectrometer). The FTIR analysis was carried out in the 400–4000 cm^{-1} wavenumbers range and a resolution of 2 cm^{-1} and 8 scans for each sample. Before analysis, all hydrogel samples (pure and with MCO and cCB) were freeze-dried. The raw data were manipulated by baseline correction, normalised, and smoothed.

Electrical properties measurements

The electrical properties of the hydrogel samples were determined based on electrochemical impedance spectroscopy (EIS) measurements using a VersaSTAT 4 potentiostat. For the measurements, hydrogel in the form of a disc was located between two nickel plates (2x15x15 mm) connected with the impedance analyser (2-probe measurement) (Figure 7). The impedance spectrum was acquired in the frequency range of 0.01 Hz – 10 kHz and at an amplitude of 10 mV. The data was analysed by the ZView software.

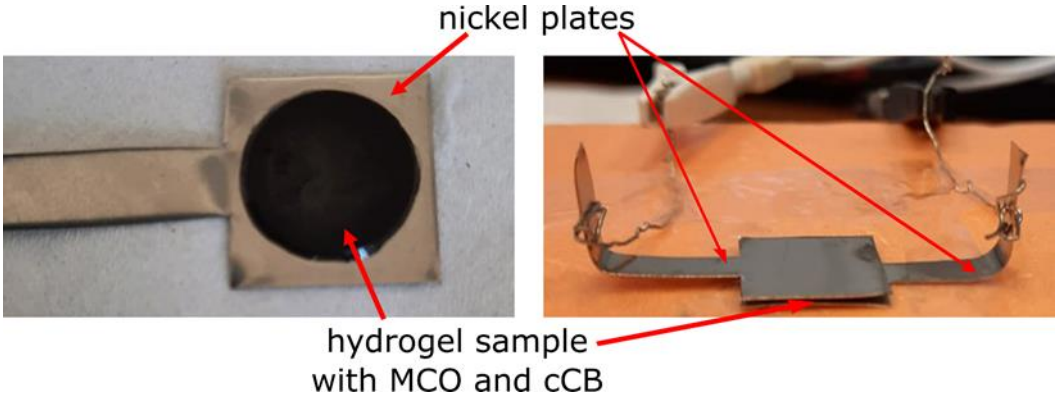

Figure 7: Electrical properties measuring system of hydrogel-based samples with catalyst (MCO) and conductive carbon black (cCB) particles.

Electrode preparation and electrochemical measurements

For the electrochemical analysis, 5 µL of hydrogel precursor solution was dropped on a rotating glassy carbon (GC) electrode with a working area of 0.196 cm^2. OER experiments were performed in a three-electrode system controlled by a BioLogic BP-300 potentiostat/impedance meter in an O2-saturated 0.1 M KOH electrolyte (Titripur®, Merc, Germany). Rotating Ring Disk Electrode (RRDE-3A) equipment was used at 1600 rpm. GC and Hg/HgO were the working electrode and the reference electrode, respectively. Linear sweep voltammetry (LSV) data were recorded from 1.1 to 2.0 V vs. RHE with a 10 mV/s scan rate. The charge transfer resistance (R_{ct}) was determined based on the EIS measurements. The spectra were obtained in the frequency range from 10 kHz to 0.1 Hz at 1.7 V vs. RHE, and with an amplitude of 10 mV. All potential values were converted to the reversible hydrogen electrode (RHE) and then iR-corrected. Cycling voltammetry (CV) scans were performed at scan rates of 10, 20, 40, 60, 80, and 100 mV s^{-1} to estimate the double-layer capacitance (C_{dl}). The non-faradaic potential region was applied (from 1 V to 1.7 V vs. RHE).

Funding

The presented research is part of the ‘Nanocrystalline ceramic materials for efficient electrochemical energy conversion’ project, carried out within the First TEAM programme of the Foundation for Polish Science (grant agreement nr. POIR.04.04.00-00-42E9/17-00).

References

1. Skelton, S.; Bostwick, M.; O’Connor, K.; Konst, S.; Casey, S.; Lee, B. P. *Soft Matter*, **2013**, 9, 3825–3833. https://doi.org/10.1039/C3SM27352K

2. Haq, M. A.; Su, Y.; Wang, D. *Mater. Sci. Eng., C*, **2017**, 70, 842–855. https://doi.org/10.1016/j.msec.2016.09.081

3. Guan, Y.; Zhang, Y. *Soft Matter*, 2011, 7, 6375-6384. https://doi.org/10.1039/C0SM01541E

4. Ahmed, E. M. *J. Advanced Research*, **2015**, 6, 105–121. https://doi.org/10.1016/j.jare.2013.07.006

5. Catoira, M. C.; Fusaro, L.; Di Francesco, D.; Ramella, M.; Boccafoschi, F. *Journal of Materials Science: Materials in Medicine*, **2019**, 30. https://doi.org/10.1007/s10856-019-6318-7

6. Rosiak, J. M.; Yoshii, F. *Nucl. Instr. and Meth. in Phys. Res.*, **1999**, 151, 56-64. https://doi.org/10.1016/S0168-583X(99)00118-4

7. Pawłowska, S. *IPPT Reports on Fundamental Technological Research*, 2018, 2, 1-106.

8. Hoffman, A. S. *Advanced Drug Delivery Reviews*, **2012**, 64, 18–23. https://doi.org/10.1016/j.addr.2012.09.010

9. Cascone, S.; Lamberti, G. *International Journal of Pharmaceutics*, **2019**, 573, 118803. https://doi.org/10.1016/j.ijpharm.2019.118803

10. Aswathy, S. H.; Narendrakumar, U.; Manjubala, I. *Heliyon*, **2020**, 6, e03719. https://doi.org/10.1016/j.heliyon.2020.e03719

11. Herrmann, A.; Haag, R.; Schedler, U. *Adv. Healthcare Mater.*, **2021**, 10, 2100062. https://doi.org/10.1002/adhm.202100062

12. Bae, J.; Park, J.; Kim, S.; Cho, H.; Kim, H. J.; Par, S.; Shin, D.-S. *Journal of Industrial and Engineering Chemistry*, **2020**, 89, 1-12. https://doi.org/10.1016/j.jiec.2020.05.001

13. Ziai, Y.; Rinoldi, C.; Nakielski, P.; De Sio, L.; Pierini, F. *Current Opinion in Biomedical Engineering*, **2022**, 24, 100413. https://doi.org/10.1016/j.cobme.2022.100413

14. Wang, Y.; Liu, H.; Ji, X.; Wang, Q.; Tian, Z.; Liu, S. *International Journal of Biological Macromolecules*, **2022**, 212, 393–401. https://doi.org/10.1016/j.ijbiomac.2022.05.154

15. Tang, S.; Liu, Z.; Xiang, X. *Carbon Lett.*, **2022**, 32, 1395–1410. https://doi.org/10.1007/s42823-022-00402-1

16. Wang, H.; Xiang, J.; Wen, X.; Du, X.; Wang, Y.; Du, Z.; Cheng, X.; Wang, S. *Composites Part A: Applied Science and Manufacturing*, **2022**, 155, 106835. https://doi.org/10.1016/j.compositesa.2022.106835

17. Jayakumar, A.; Jose, V. K.; Lee, J.-M. *Small Methods*, **2020**, 4, 1900735. https://doi.org/10.1002/smtd.201900735

18. Mishra, S.; Rani, P.; Sen, G.; Dey, K. P. In: Thakur, V., Thakur, M. (eds) Hydrogels. Gels Horizons: From Science to Smart Materials. *Springer*, **2018**, 145–173. https://doi.org/10.1007/978-981-10-6077-9_6

19. Kim, J. M.; Kim, J.-H.; Kim, J.; Lim, Y.; Kim, Y.; Alam, A.; Lee, J.; Ju, H.; Ham, H. C.; Kim, J. Y. *Adv. Mater.*, **2020**, 2002210, 1-24. https://doi.org/10.1002/adma.202002210

20. Lu, X.; Zhao, C. *Nat Commun*, **2015**, 6, 6616. https://doi.org/10.1038/ncomms7616

21. Zhanga, W.; Fenga, P.; Chena, J.; Suna, Z.; Zhao, B. *Progress in Polymer Science*, **2019**, 88, 220–240. https://doi.org/10.1016/j.progpolymsci.2018.09.001

22. Cai, J.; Zhang, X.; Liu, W.; Huang, J.; Qiu, X.. *; Polymer,* **2020**, 122643. https://doi.org/10.1016/j.polymer.2020.122643

23. Baei, P.; Jalili-Firoozinezhad, S.; Rajabi-Zeleti, S.; Tafazzoli-Shadpour, M.; Baharvand, H.; Aghdami, N. *Materials Science and Engineering: C,* **2016**, 63, 131–141. https://doi.org/10.1016/j.msec.2016.02.056

24. Xiang, Y.; Chen, D. *European Polymer Journal,* **2007**, 43, 4178–4187. https://doi.org/10.1016/j.eurpolymj.2007.08.005

25. Park, J.; Jeon, J.; Kim, B.; Lee, M. S.; Park, S.; Lim, J.; Yi, J.; Lee, H.; Yang, H. S.; Lee, J. Y. *Adv. Funct. Mater.*, **2020**, 30, 2003759. https://doi.org/10.1002/adfm.202003759

26. Gao, H.; Sun, Y.; Zhou, J.; Xu, R.; Duan, H. *ACS Applied Materials & Interfaces*, **2013**, 5, 425–432. https://doi.org/10.1021/am302500v

27. Cui, Z.; Zhou, M.; Greensmith, P. J.; Wang, W.; Hoyland, J. A.; Kinloch, I. A.; Freemont, T.; Saunders, B. R. *Soft Matter,* **2016**, 12, 4142–4153. https://doi.org/10.1039/C6SM00223D

28. Shi, Y.; Pan, L.; Liu, B.; Wang, Y.; Cui, Y.; Bao, Z.; Yu, G. *J. Mater. Chem. A,* **2014**, 2, 6086–6091. https://doi.org/10.1039/C4TA00484A

29. Wu, Y.; Chen, Y. X.; Yan, J.; Yang, S.; Dong, P.; Soman, P. *Journal of Materials Chemistry B,* **2015**, 3, 5352–5360. https://doi.org/10.1039/C5TB00629E

30. Rinoldi, C.; Lanzi, M.; Fiorelli, R.; Nakielski, P.; Zembrzycki, K.; Kowalewski, T.A.; Urbanek, O.; Grippo, V.; Jezierska-Woz, K.; Maksymowicz, W.; Camposeo, A.; Bilewicz, R.; Pisignano, D.; Sanai, N.; Pierini, F. *Biomacromolecules*, **2021**, 22, 3084-3098. https://doi.org/10.1021/acs.biomac.1c00524.

31. Mawad, D.; Lauto, A.; Wallace, G. G. Conductive Polymer Hydrogels. In: Kalia, S. (eds) Polymeric Hydrogels as Smart Biomaterials. Springer Series on Polymer and Composite Materials. Springer, Cham., 2016. https://doi.org/10.1007/978-3-319-25322-0_2

32. Zhanga, W.; Fenga, P.; Chena, J.; Suna, Z.; Zhao, B. *Progress in Polymer Science*, **2019**, 88, 220–240. https://doi.org/10.1016/j.progpolymsci.2018.09.001

33. Chen, S.; Duan, J.; Jaroniec, M.; Qiao, S. Z. *Angew. Chemie - Int. Ed.*, **2013**, 52, 13567–13570. https://doi.org/10.1002/anie.201306166.

34. Divya Madhuri, U.; Radhakrishnan, T. P. *ChemElectroChem*, **2019**, 6, 1984–1989. https://doi.org/10.1002/celc.201801659.

35. Guo, Y.; Bae, J.; Fang, Z.; Li, P.; Zhao, F.; Yu, G. *Chem. Rev.*, **2020**, 120, 7642–7707. https://doi.org/10.1021/acs.chemrev.0c00345

36. Rong, Q.; Lei, W.; Liu, M. *Chem. Eur. J.*, **2018**, 24, 16930-16943. https://doi.org/10.1002/chem.201801302

37. Zhou, C.; Wu, T.; Xie, X.; Song, G.; Ma. X.; Mu, Q.; Huang, Z.; Liu, X.; Sun, C.; Xu, W. *European Polymer Journal*, **2022**, 177, 111454. https://doi.org/10.1016/j.eurpolymj.2022.111454

38. Yang, R.; Chen, X.; Zheng, Y.; Chen, K.; Zeng, W.; Wu, X. *J. Mater. Chem. C*, **2022**, 10, 5380. https://doi.org/10.1039/D1TC06162C

39. Hong, Y.; Lin, Z.; Yang, Y.; Jiang, T.; Shang, J.; Luo, Z. *Int. J. Mol. Sci.*, **2022**, 23, 4578. https://doi.org/10.3390/ijms23094578

40. Walker, B. W.; Portillo Lara, R.; Mogadam; E.; Hsiang Yu, C.; Kimball, W.; Annabi, N. *Progress in Polymer Science*, **2019**, 92, 135-157.

41. Xu, Y.; Patino Gaillez, M.; Rothe, R.; Hauser, S.; Voigt, D.; Pietzsch, J.; Zhang, Y. *Adv. Healthcare Mater.*, **2021**, 10, 2100012. https://doi.org/10.1002/adhm.202100012

42. Pawłowska, S.; Rinoldi, C.; Nakielski, P.; Ziai, Y.; Urbanek, O.; Li, X.; Kowalewski, T. A.; Ding, B.; Pierini, F. *Adv. Mater. Interfaces*, **2020**, 7, 2000247. https://doi.org/10.1002/admi.202000247

43. Qu, J.; Liang, Y.; Shi, M.; Guo, B.; Gao, Y.; Yin, Z. *International Journal of Biological Macromolecules*, **2019**, 140, 255-264. https://doi.org/10.1016/j.ijbiomac.2019.08.120

44. Qu, J.; Zhao, X.; Ma, P. X.; Guo, B. *Acta Biomaterialia*, **2018**, 72, 55–69. https://doi.org/10.1016/j.actbio.2018.03.018

45. Bansal, M.; Dravid, A.; Aqrawe, Z.; Montgomery, J.; Wu, Z.; Svirskis, D. *Journal of Controlled Release*, **2020**, 328, 192-209. https://doi.org/10.1016/j.jconrel.2020.08.051

46. Madhuri, U. D.; Radhakrishnan, T. P. *J. Phys. Chem. C*, **2019**, 124, 44–51. https://doi.org/10.1021/acs.jpcc.9b08739

47. Nakielski, P.; Pawłowska, S.; Rinoldi, C.; Ziai, Y.; Sio, L. De; Urbanek, O.; Zembrzycki, K.; Pruchniewski, M.; Lanzi, M.; Salatelli, E.; Calogero, A.; Kowalewski, T. A.; Yarin, A. L.; Pierini, F. *ACS Appl. Mater. Interfaces*, **2020**, 12, 54328–54342. https://doi.org/10.1021/acsami.0c13266

48. Pawłowska, S.; Lankauf, K.; Błaszczak, P.; Karczewski, J.; Górnicka, K.; Cempura, G.; Jasiński, P.; Molin, S. *Applied Surface Science*, **2023**, 619, 156720. https://doi.org/10.1016/j.apsusc.2023.156720

49. Katsumoto, Y.; Tanaka, T.; Sato, H.; Ozaki, Y. *The Journal of Physical Chemistry A*, **2002**, 106, 3429–3435. https://doi.org/10.1021/jp0124903

50. Sriram, B.; Baby, J. N.; Hsu, Y.-F.; Wang, S.-F.; Joseph, X. B.; George, M.; Veerakumar, P.; Lin, K. C. *ACS Appl. Electron. Mater.* , **2021**, 3, 3915–3926. https://doi.org/10.1021/acsaelm.1c00506

51. Shanmugavalli, V.; Vishista, K. *SN Applied Sciences*, **2020**, 2, 683. https://doi.org/10.1007/s42452-020-2046-3

52. Wu, Y.; Chen, Y. X.; Yan, J.; Quinn, D.; Dong, P.; Sawyer, S. W.; Soman, P. *Acta Biomaterialia*, **2016**, 33, 122–130. https://doi.org/10.1016/j.actbio.2016.01.036

53. Al-Mossawi, M.; Warren, H.; Molino, P.J.; Calvert, P.; Panhuis, M. *Mater. Adv.*, **2021**, 2, 1369-1377. https://doi.org/10.1039/D0MA00985G

54. Yang, B.; Yao, F.; Hao, T.; Fang, W.; Ye, L.; Zhang, Y.; Wang, Y.; Li, J.; Wang, C. *Adv. Healthcare Mater.*, **2016**, 5, 474–488. https://doi.org/10.1002/adhm.201500520

55. Shay, T.; Velev, O. D.; Dickey, M. D. *Soft Matter*, **2018**, 14, 3296-3303. https://doi.org/10.1039/C8SM00337H

56. Yang, J.; Wang, X.; Li, B.; Ma, L.; Shi, L.; Xiong, Y.; Xu, H. *Adv. Funct. Mater.*, **2017**, 27, 1606497. https://doi.org/10.1002/adfm.201606497.

57. Tang, C.; Thomas, B.; Ramírez-Hernández, M.; Mikmeková, E. M.; Asefa, T. *ACS Appl. Mater. Interfaces*, **2022**, 14, 20919–20929. https://doi.org/10.1021/acsami.2c01667

58. Lankauf, K.; Cysewska, K.; Karczewski, J.; Mielewczyk-Gryń, A.; Górnicka, K.; Cempura, G.; Chen, M.; Jasiński, P.; Molin, S. *International Journal of Hydrogen Energy*, **2020**, 45, 14867-14879. https://doi.org/10.1016/j.ijhydene.2020.03.188

59. Anantharaj, S.; Karthik, P. E.; Kundu, S. *J. Mater. Chem. A*, **2015**, 3, 24463–24478. https://doi.org/10.1039/c5ta07075a

60. Ono, Y.; Shikata, T. *J. Am. Chem. Soc.*, **2006**, 128, 10030–10031. https://doi.org/10.1021/ja063990i

61. Du, H.; Wickramasinghe, R.; Qian, X. *J. Phys. Chem. B*, **2010**, 114, 16594–16604. https://doi.org/10.1021/jp105652c

62. Deshmukh, S.; Mooney, D. A.; McDermott, T.; Kulkarni, S.; Don MacElroy, J. M. *Soft Matter*, 2009, 5, 1514.